3-24-2016

Modulation of Whole Cell Currents in Human Neuroblastoma Cells via the Hormone Aldosterone: An *in vitro* Study

Harish Kumar Chittam

Modulation of Whole Cell Currents in Human Neuroblastoma Cells via the Hormone Aldosterone: An *in vitro* Study

by

Harish K. Chittam

A thesis submitted in partial fulfillment
of the requirements for the degree of
Master of Science in Biomedical Engineering
Department of Chemical and Biomedical Engineering
College of Engineering
University of South Florida

Co-Major Professor: Joseph P. Walton, Ph.D.
Co-Major Professor: Venkat R. Bhethanabotla, Ph.D.
Robert D. Frisina, Ph.D.

Date of Approval:
March 21, 2016

Keywords: Bumetanide, Patch Clamp, Ion Channels, K^+ Currents, Micropipette

DEDICATION

I would like to dedicate this thesis to my family, Manik, Aru and Akhil along with my teachers for being a tremendous source of inspiration and knowledge.

ACKNOWLEDGMENTS

I would like to express my deep gratitude to my advisor Dr. Walton for his enormous guidance and support throughout my research. His expertise and experience served at every stage of this research from idea to final product. Equally important advice and support is provided by Dr. Venkat and I'm greatly thankful to him, this work would not be possible without him.

I'm very grateful to Dr. Frisina for believing in me and supporting me since day one, I've gained immense amount of knowledge and wisdom under his supervision. Special thanks to my colleague and friend Parveen, who not only gave invaluable suggestions, but also hours of time on every day discussions.

I would like to thank Drs. Bo Ding and Xia Xiao Zhu for helping me learn the essential skills and providing all the inputs at each stage. I also thank Shannon Salvog for her assistance in getting all the needed approvals and laboratory equipment.

Finally, I would like to thank all of my friends, colleagues, and family members for their moral support and encouragement through all the difficult times.

TABLE OF CONTENTS

LIST OF TABLES

LIST OF FIGURES

ABSTRACT

Ion channels play a critical role in maintaining homeostasis by moving various ions in and out of cells. The Na^+-K^+-$2Cl^-$ or NKCC1 ion channel is involved in the regulation of Na^+, K^+, and Cl^- across cell membranes, and plays a key role in many forms of cellular physiology. In the cochlea, NKCC1 is involved in endolymph production and maintenance of the endocochlear potential. Our hypothesis is that blocking NKCC1 channels should directly impact auditory sensitivity causing hearing loss. Our lab has also shown that the hormone aldosterone (ALD) can upregulate NKCC1 protein expression *in vitro* and *in vivo.* In the present investigation, we use electrophysiology and molecular biology techniques to study the biophysical mechanisms underlying the action of ALD *in vitro* on NKCC1 in the SH-SY5Y cell line. Our initial protein expression studies using RT-PCR found that proteins specific to NKCC1channels were present in SH-SY5Y neuronal cells. Whole cell currents measured using patch clamp methodology, were used to analyze the effects of various compounds on NKCC1 in the SH-SY5Y cell line. Control data were collected under perfusion of extracellular solution (ECS), then ECS containing 10µM bumetanide was applied, and, finally a washout condition completed the experiment. Similar experiments were conducted using ALD, and we observed an increase in K^+ currents when bumetanide as well as when ALD was applied. This is the first report that indicates that ALD can directly regulate K^+ channels in SH-SY5Y cells.

CHAPTER 1:

INTRODUCTION AND BACKGROUND

1.1 NKCC1 and its Role in Inner Ear Function

As people get older, they lose their hearing ability. Apart from normal aging there are a number of other factors which contribute to this age-related hearing loss (ARHL). Recently, Na^+-K^+-$2Cl^-$ co-transport protein (NKCC1) activity was shown to be involved in age-related hearing loss [1]. $Na^+/K^+/Cl^-$ co-transporters are members of the electroneutral cation-chloride cotransporter family with two isoforms, the secretory isoform and absorptive isoform found in exocrine epithelia and the renal thick ascending limb of Henle's loop, respectively [2]. In the plasma membrane, NKCC1 exists as an oligomer and the dominant structural unit of NKCC1 is a homodimer of 355kDa [3]. NKCC1 carries out many vital functions in organs such as kidney, brain and cochlea. For instance, NKCC1 has key a role in reducing GABAergic inhibition in spontaneously hypertensive rats through chloride homeostasis disruption [4]. Low intracellular Cl^- ion concentration and protein phosphatase inhibition promotes phosphorylation of NKCC1 and thus activates it. In addition, NKCC1 transports chloride ions into the cell, driven energetically across the membrane because of gradients between Na^+ and/or K^+ and Cl^- ions [5].

The population with ARHL continues to grow, as the "Baby Boomers" reach retirement ages, and understanding the underlying mechanisms of age-related changes in cochlear function will be key for developing potential therapies. ARHL occurrence can be altered via both genetically inherited traits and also by exposure to loud noise or ototoxic drugs [6, 7].

Schuknecht classified ARHL into four types i.e., sensory, neural, cochlear-conductive and strial. Strial ARHL occurs due to degeneration of the stria vascularis, which is a specialized organ located on the lateral wall of the cochlear scala media [8, 9]. Age-linked stria vascularis degeneration has been associated as a primary cause of presbycusis or ARHL [8, 9].

The endocochlear potential (EP) is the voltage difference established by cells in the stria vascularis and is crucial for the normal functioning of inner ear receptor cells [10]. A high resting EP is established due to high K^+ and low Na^+ concentration in endolymph [6]. Application of the NKCC1 antagonist furosemide decreases the EP and also elevates the thresholds of auditory nerve fibers [11]. The EP declines with age, and in addition down regulation or inactivation of NKCC1 membrane proteins causes decreases in EP. Therefore it's evident that NKCC1 plays a crucial role in ARHL. When an acoustic stimulus reaches stereocilia of the inner ear, K^+ ions are transported from endolymph into the hair cell, causing depolarization of the hair cell membrane. Electrical signals generated following depolarization are transported to the brain through the auditory nerve [12]. In stria marginal cells of the cochlea, NKCC1 participates in production of a potassium-rich endolymphatic fluid [1]. Decreases in endolymph K^+ concentration leads to significant hearing deficits, which indicates the importance of the physiological role of NKCC1 in the peripheral auditory system [13].

There are both antagonists and agonists to NKCC1 that can alter its function and could serve as possible therapeutic agents. One such antagonist is bumetanide which is a diuretic and a specific blocker of NKCC1 [1, 14]. Bumetanide has approximately a 500-fold greater affinity to NKCC1, compared to potassium-chloride transport member 5 (KCC2) [15]. In some cellular assays, bumetanide in low concentrations (2-10μM) can inhibit NKCC1 and is an ideal tool to study NKCC1 physiological actions [15]. Aldosterone (ALD), a naturally occurring hormone, is

considered an agonist of NKCC1, and plays an important role in the maintenance of Na^+, K^+ and acid-base balance in renal systems [1]. In aging and many other disease conditions, decreases in NKCC1 activity or/and mis-regulation of Na^+ and K^+ occurs [1].

1.2 Motivation

Previous work in our lab has shown that long-term systemic treatment of ALD has restored hearing in aging mice, probably by increasing stria sodium-potassium transport and up-regulation of NKCC1 protein expression through mineralocorticoid receptors [1, 16]. This provides motivation for us to investigate the effects of ALD on NKCC1 and the underlying cellular and molecular events taking place. Our objective in using whole-cell patch clamp recordings is to study the electrical changes of NKCC1 and other ion channels following application of ALD and its antagonists. In the present investigation, we recorded whole-cell currents from SH-SY5Y cells, as these cells are derived from a neuronal cell line.

1.3 Thesis Organization

This thesis is comprised of four chapters. Chapter one provides an introduction to NKCC1 and its roles in the auditory system and motivation of this research. Chapter two describes the materials and methods used to carry out this research. Chapter three contains the results and discussion, accompanied by figures, and chapter four discusses the implication of our findings and describes future work.

CHAPTER 2:

MATERIALS AND METHODS

2.1 Reagents and Equipment

Chemicals required for extracellular and intracellular solutions including NaCl, KCL, Glucose, $MgCl_2$, $CaCl_2$ and $MgSO_4$ were obtained from Fischer Scientific Company, LLC (Pittsburg, PA). HEPES ((2-Hydroxyethyl) piperazine-1-ethanesulfonic acid sodium salt, N-(2-Hydroxyethyl) piperazine-N′-(2-ethanesulfonic acid)), Adenosine 5'-triphosphate magnesium salt, EDTA were purchased from Sigma-Aldrich, Inc. (St. Louis, MO). DMEM, F12 reagents for cell culture were obtained from Gibco Life technologies, LLC (Carlsbad, CA) and the RT-PCR kit for protein expression was purchased from Invitrogen (Carlsbad, CA).

Instruments used in making extracellular and intracellular solutions were a Mettler Toledo balance for weighing chemicals, and Beckman ISE meter for pH measurements. A Thermo 1300 series A2 Biological safety cabinet, VWR Incubator and Nikon eclipse TS100 microscopy were used for cell culture. Molecular devices (Molecular Devices, LLC. Sunnyvale, CA) supplied the patch clamp amplifier Multiclamp 700B, and the DMI 4000 phase contrast microscopy used to visualize the cells was performed with a Leica Microsystems (Leica Microsystems, Inc. Buffalo Grove, IL). Micromanipulators were obtained from Warner instruments, LLC. (Hamden, CT).

2.1.1 Patch Clamp Setup

Patch clamp is one of the most highly sensitive and challenging techniques used in neuroscience, because of this it is crucial to follow standard procedures. Electrical and vibration interference are the two main variables to be considered in setting up a patch clamp system. These two parameters are crucial, because while performing experiments, significant noise can be introduced from electrical and vibrational interference [17]. To reduce electrical noise a Faraday cage was used to shield the setup from unwanted electrostatic discharges and electric fields. The microscope, pre-amplifiers and manipulators were placed inside the cage and all the devices were grounded. External vibrations were compensated by using a Micro-g anti-vibration table (model no 63-533, TMC, Peabody, MA) where the table top is mounted on a gas source (nitrogen tank).

2.1.1.1 Microscope

A Leica DMI 400B inverted microscope was used in our patch clamp system to visualize the cells at 5x, 10x, 20x, and 40x magnification. A condenser is present on the top of the recording chamber and the distance between the condenser and the recording chamber is crucial, as it allows enough space for the micropipette to access the recording chamber. A Nikon camera was connected to the microscope which is in turn connected to a computer which allows for capturing video and photos.

2.1.1.2 Amplifiers

Amplifiers included a measuring amplifier and clamping amplifier. Measuring amplifiers have an extension called the external probe and the recording electrode that makes contact with

the cell is connected to the probe through a pipette holder. The Multiclamp 700B amplifier receives data from the measuring amplifier and acquires the data via a Multiclamp software user interface.

2.1.1.3 Manipulators

Micromanipulators (Warner Instruments, Hamden, CT) placed inside the Faraday cage were used to move the probe precisely. The primary function of the manipulators was to position the micropipettes near the cell.

2.1.1.4 Pipette Puller and Patch Pipettes

Microelectrodes were fabricated on a Sutter Instruments model-97 pipette puller (Novato, CA) programmed with pressure, temperature and velocity parameters in order to get the desired pipette tip size and resultant resistance of 5-8 MΩ. Warner instrument glass electrodes were used to make patch pipettes and were prescreened under a microscope to select the desired shape.

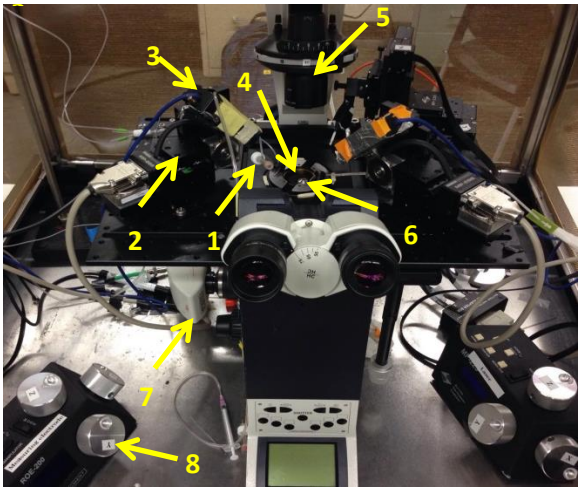

Figure 2.1: (a) Patch clamp system and its main components. (1) Pipette holder, (2) Manipulator, (3) Preamplifier, (4) Objective lens, (5) Condenser, (6) Recording chamber, (7) Microscope camera and (8) Manipulator controller. (b) Data Acquisition unit, DigiData 1440A. (c) Multiclamp 700B amplifier.

Figure 2.1: (Continued)

2.2 Cell Culture

SH-SY5Y (ATCC® CRL-2266™) neuroblastoma cells were cultured in a medium containing a mixture of F12 & DMEM (1:1 v/v) supplemented with 1% Penicillin Streptomycin

(Pen Strep) and 10% FBS. The cells were then incubated in an incubator maintained at 37^{o}C temperature, 5% CO_2 and 95% humidity. Over the past four decades, only a little change occurred in normal cell culture conditions of SH-SY5Y [18]. The doubling time for parental populations was approximately 27 h and the medium was replaced after every 4-7 days. Cells were incubated with trypsin solution for 1-2 minutes to detach adherent cells. Cells with trypsin solution were combined with equal volume of F12 & DMEM (1:1 v/v) medium with 1% Pen Strep and 10% FBS added to it. The resultant solution was then centrifuged at 1500 rpm for 5 min. The pellets were then suspended in F12 & DMEM (1:1 v/v) medium with 1% Pen Strep and 10% FBS. The cells at this stage are undifferentiated and appear round and form clusters. Previously, it was reported that the undifferentiated cells lack mature neuronal markers and have the ability to proliferate continuously [18]. Morphologically, the undifferentiated cells were neuroblast-like with non-polarized cell bodies and few truncated processes.

Differentiation of SH-SY5Y cells is achieved by adding retinoic acid (RA) to the cell culture medium. RA has known to possess cellular differentiation and growth inhibiting properties [19, 20]. Within 48h of plating, the serum-containing medium was replaced with neurobasal medium supplemented with B27 and GlutaMAX. To promote differentiation, 10μM all-trans-retinoic acid was added to the cell culture medium and the medium was replaced after every 48h. Differentiated cells were observed under the microscopy and were more pyramidal shaped, distributed, and had extended neurites (Figure 2.2).

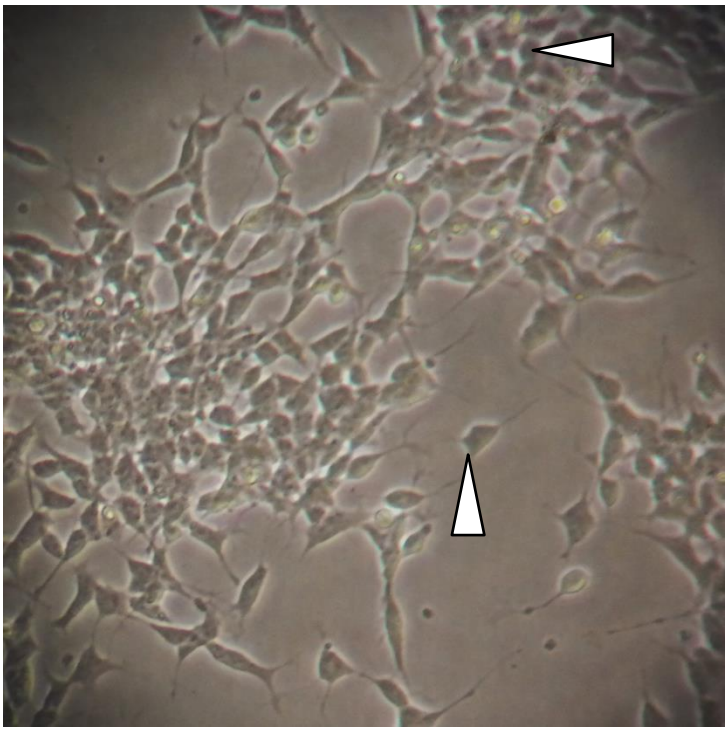

Figure 2.2: SH-SY5Y cells observed under bright field microscopy (Nikon Eclipse) using 20x magnification. Top arrow displays undifferentiated (S-type) clumps of cells growing on top of one another and bottom arrow displays differentiated SH-SY5Y cells with extended neurites referred to as N-type cells.

2.3 RT-PCR Experiments

2.3.1 RNA Isolation

Undifferentiated and differentiated SH-SY5Y cells total RNA was extracted according to the RNAeasy Mini kit (Qiagen, Inc. Valencia, CA) instructions. Initially, the cell culture medium was discarded completely and cells were lysed using a rubber policeman in the petri dishes by adding 350 μl of RLT buffer. The lysate was then homogenized for 30 s using a rotor-stator homogenizer. One volume of 70% ethanol was then added to lysate and mixed well using pipette. Contents were then transferred to RNeasy column and centrifuged at 10000 rpm for 15 s, and the flow through obtained was discarded. 350 μl of RW1 buffer was added to the RNeasy

column, followed by centrifugation for 15 s at 10000 rpm, with the flow through discarded. A mixture of 10 μl DNAase stock I solution with 70 μl of RDD buffer was prepared and then transferred to the RNeasy column membrane and placed on a benchtop for 15 min at a temperature of 26^{o}C. In the next step, 350 μl of RW1 buffer was added to the RNeasy column, followed by centrifugation at 10000 rpm for 15 s and the flow through obtained was discarded. Then, 700 μl of RW1 buffer was added, followed by centrifugation for 15 s at 10000 rpm, with the flow through discarded. Then 500 μl of RPE buffer was added, followed by centrifugation for 15 s at 10000 rpm, and the flow through obtained discarded. The previous step was repeated with centrifugation duration extended to 2 min. The RNeasy column was then placed in a collection tube and 30 µl of RNase free water added, followed by centrifugation for 1 min at 10000 rpm. The final RNA yield is collected and used in the RT-PCR assay.

2.3.2 RT-PCR

Quantitative reverse-transcription-polymerase chain reaction was performed in a two-step approach: first qRT-PCR was done using Enhanced Avian HS RT-PCR-100 Kit (HSRT20; Sigma) and then Real-time PCR using SYBR Green PCR Master Mix (7900HT; Applied Biosystems, Carlsbad CA). RT-PCR was performed according to manufacturer's procedure and primers set details are given in the table below.

Table 2.1: Primer sequences and their details.

	Targets		Primer Sequence	Product size (bp)
RT-PCR	NKCC1	S	5'-ACCTTCGGCCACAACACCATGGA-3'(S)	184 kbp
		AS	5'-ACCACAGCATCTCTGGTTGGA-3' (AS)	

S – Sense strand, AS- Antisense strand

Initially, semiquantitative qRT-PCR reaction was performed at 45^{o}C for 50 min, and the reaction conditions were adjusted to eliminate competition between primer sets. The products obtained from primer reaction were then PCR amplified. First cycle conditions were 95^{o}C for 10min, 65^{o}C for 45 s and 72^{o}C for 1 min followed by 25 cycles at 95^{o}C for 45 s, 65^{o}C for 45 s, and 72^{o}C for 1 min. Negative control was performed which included RNA instead of cDNA [1].

Using qRT-PCR products and SYBR Green PCR Master Mix, real-time RT-PCR mixture was prepared. The conditions for thermo cycling conditions were same as the semiquantitative reaction. In each PCR reaction negative and also positive samples were included. The expression of gene was referred to the β-actin mRNA content.

2.4 Electrophysiological Recordings

2.4.1 Preparation of Extracellular and Intracellular Solutions

Standard extracellular solution (ECS) and intracellular solution (ICS) were prepared using the concentrations described in Table 2.2. Weight of each component was calculated using the concentration, molecular weight and final volume. All the contents were sterilized using an autoclave at 15 psi pressure, 121^{o}C temperature for 20 min. To prevent degradation, glucose was added to ECS after sterilization. In preparation of ICS solution Mg ATP was added after autoclave sterilization. For ECS the pH was adjusted to 7.3 using NaOH and for ICS pH was adjusted to 7.4 using KOH.

Table 2.2: ECS & ICS components and their concentrations for SH-SY5Y cells.

ECS		ICS	
Components	**Concentration (mM)**	**Components**	**Concentration (mM)**
NaCl	125	KCl	140
KCL	4	NaCl	4
$CaCl_2$	2	$CaCl_2$	0.02
$MgSO_2$	1.2	EGTA	0.8
Glucose	10	$MgCl_2$	2
HEPES	10	MgATP	4
		HEPES	10

2.4.2 Perfusion System

A customized perfusion system was constructed to allow local application of drugs to cells and continuous exchange of ECS. Our perfusion system is comprised of syringe reservoirs, luer stopcocks, blunt-end needles, polyethylene tube (PE -160), and 4-1 manifold, all of them were purchased from Warner Instruments (Hamden, CT). The syringe reservoirs were positioned at a fixed height from the recording chamber using a retort stand through a 3D printed holder. Syringe openings are connected to luer stopcocks and the open end of luer stopcocks are connected to blunt end needles. PE tubing connects blunt end needles to manifold inputs and number of reservoirs should be equal to number of manifold inputs. A single tube exits the manifold and goes into the petri dish.

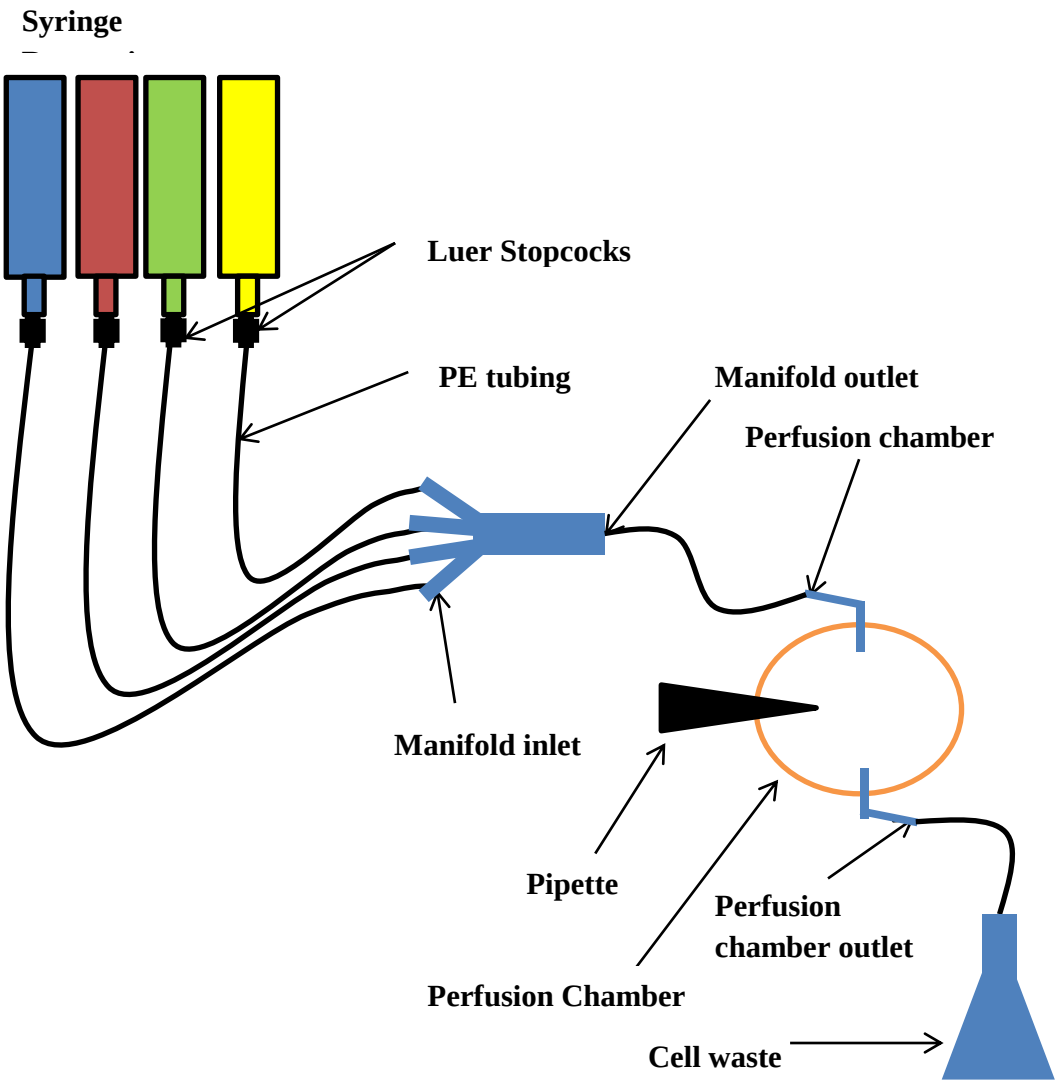

Figure 2.3: Schematic diagram representing various components of the gravity fed perfusion system. The system was comprised of syringe reservoirs, where different solutions can be loaded in each reservoir. The bottom ends of the syringes were connected to luer stopcocks, which were then connected to PE tubing through blunt needles. The other end of the PE tubes went into the manifold inlets, and the manifold outlet was connected to the perfusion chamber inlet through PE tube. The perfusion chamber outlet was then connected to the cell waste container through PE tubing.

2.4.3 Micropipette

For whole-cell recordings micropipettes were prepared using a Flame/brown micropipette puller (Model-97, Shutter Instruments Co. Novato, CA). Initially, fire polished Borosilicate

glass pipettes were positioned in the pipette puller and pulling parameters (pressure, temperature, and velocity) were adjusted to achieve desired pipette resistance of 5-8 MΩ. The tip of the micropipette was then examined under Olympus BH2 upright microscopy (Olympus America, Inc., Center Valley, CA) to ensure it had a stubby tapered end.

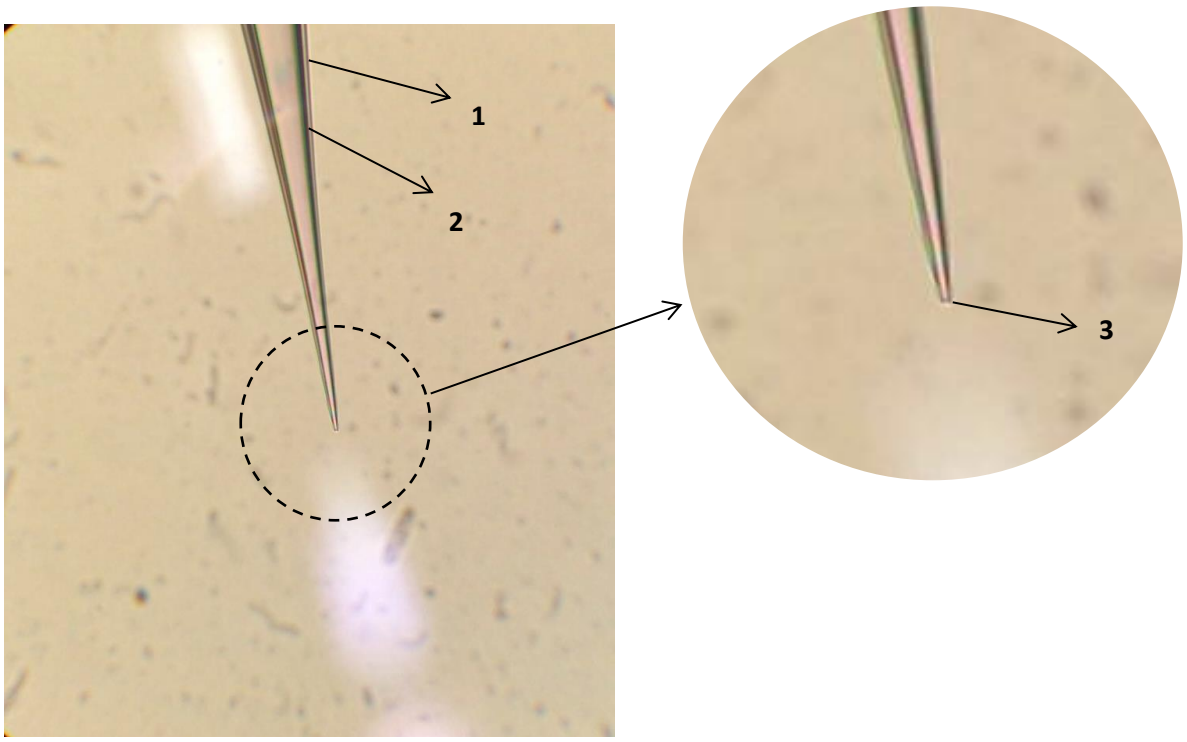

Figure 2.4: Optimal micropipette shape for whole cell recording, examined under Olympus BH2 microscopy at 40x magnification. The inset is magnified and shown, (1) Pipette (2) Taper and (3) Tip.

2.4.4 Whole Cell Recording

Initially, the cell culture medium present in the petri dish is replaced with ECS and placed in the recording chamber. The chamber inlet and outlet are adjusted in such a way that the inlet groove is completely immersed in the ECS and the outlet is positioned at 45^{o} angle. The ground electrode was carefully placed in the dish ensuring that the electrode is continuously in contact with the ECS. ICS was used to fill up to three-fourth of micropipette and carefully inserting the

Ag wire into the pipette, ensure the Ag wire is in contact with the ICS. Intracellular solution contained the following components (in mM): KCl 140; NaCl 4; $CaCl_2$ 0.02; EGTA (Ethylene glycol-bis(2-aminoethylether)-*N,N,N′,N′*-tetraacetic acid) 0.8; $MgCl_2$ 2; MgATP 4; HEPES 10; pH was adjusted to 7.4 with KOH [21]. Two reservoirs were fixed to perfusion system; one filled with ECS and the other filled with ECS+Bumetanide in initial experiments and ECS+ALD in later experiments. The extracellular recording solution for SH-SY5Y contained the following (in mM): NaCl 139; KCl 4; $CaCl_2$ 2; $MgSO_4$ 1.2; D-Glucose 10; HEPES (4-(2-Hydroxyethyl) piperazine-1-ethanesulfonic acid, N-(2-Hydroxyethyl) piperazine-N′-(2-ethanesulfonic acid)) 10 and pH was adjusted to 7.3 with NaOH [21]. ECS perfusion was initiated by turning on syringe reservoir's stopcock and suction was applied to chamber outlet. Gravity aided in maintaining the continuous perfusion flow, and flowrate was controlled using a control valve.

All the recordings were performed using whole-cell patch clamp configuration at room temperature (21±1) [22]. Clampex10.3 (Molecular Devices, LLC. Sunnyvale, CA) version of software was used for recording and acquisition, and Multiclamp software was used for stimulation. Micropipettes having resistance in the range of 5-8 MΩ were selected for recording. Pipette capacitance (C_p) was negated by performing capacitance compensation prior to gigaseal formation. First the pipette was placed against the cell membrane and a Gigaseal was achieved by applying a small suction. Further negative pressure led to whole-cell configuration causing rupture of cell membrane [23]. Once a neuron was isolated recordings were digitized at 50 kHz, low pass filtered at 5 kHz and an initial holding potential was set at -60 mV. In voltage clamp mode, the currents were recorded using a range of +30 mV to -60 mV holding potential at increments of 10 mV.

Baseline whole-cell recordings were done by perfusion of ECS (with no drugs) and then ECS containing 10µM bumetanide was applied to cells and whole cell currents were recorded. Finally recordings were acquired for washout by switching back to ECS. Recordings were carried out after every ~5 min from the control recording. The flow rate of the perfusion was kept consistent at a rate of 1 ml/min. All the recordings i.e., control, bumetanide and washout were acquired from single cell each time. When switching to different solutions during recording, we ensured to keep the perfusion rate consistent. Similar experiments were conducted to study the effects of 0.1, 1 and 10 µM ALD on these cells and whole-cell current recordings were performed on several cells. Whole-cell currents had a sampling frequency of 10 KHz with an interval of 100 µs and low pass filtered at 1000 Hz using Gaussian type. These recordings were later analyzed by using I-V curves and raw patch clamp data.

CHAPTER 3:

RESULTS AND DISCUSSION

3.1 NKCC1 Co-transporter Expression in SH-SY5Y Cells

SH-SY5Y cell lines are known to express human-specific proteins and other protein isoforms [18]. To study NKCC1 gene expression in the SH-SY5Y cell line we performed a two-step RT-PCR experiment. HT-29 cells served as the control, as other studies have shown NKCC1 existence and activity in these cell lines [1] [24]. The protein expression profile shown in Figure: 3.1 also indicates the presence of NKCC1 cotransporter in SH-SY5Y cells. Markers indicated that the NKCC1 target sequence falls in the 150-200 bp size range. Using NKCC1 published sequences (NM_001046) and primers we found the amplified product length to be 184 bp, covering base pairs from 799 – 983. All four samples of SH-SY5Y cellular lysates showed a single band, of which two samples were from differentiated SH-SY5Y cells and other two from undifferentiated cells. Interestingly, both undifferentiated and differentiated cells showed the expression of NKCC1, as indicated by the bands in Figure 3.1. In sum, our findings suggest that SH-SY5Y neuroblastoma cells show the same level of NKCC1 expression in differentiated and undifferentiated states.

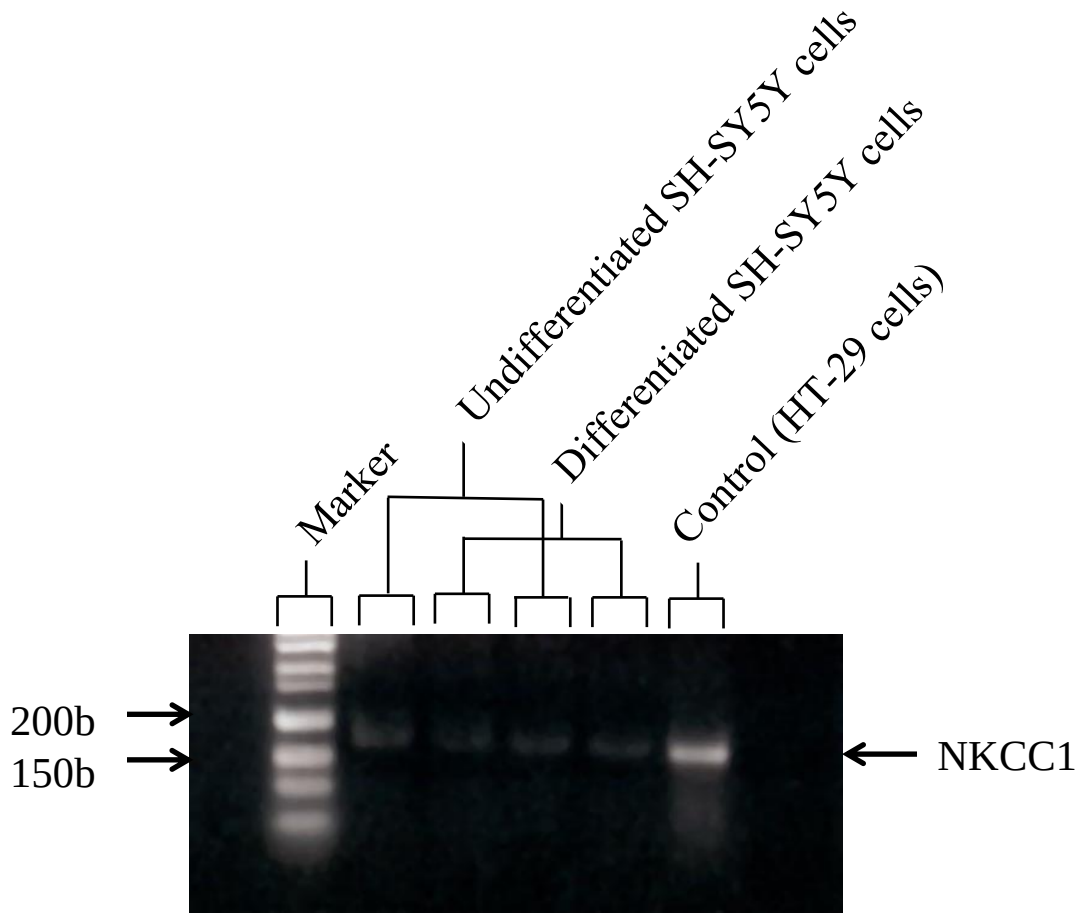

Figure 3.1: NKCC1 cotransporter is expressed in SH-SY5Y cells. Cellular lysates obtained from SH-SY5Y cells were analyzed using gel electrophoresis. Series of clear bands on left side are markers and single clear band on right side is control (HT-29 cells). NKCC1 co-transporter expression was detected at around 175 bp size in all four samples.

3.2 Bumetanide Increases K^+ Currents in SH-SY5Y Cells

Whole cell recordings were performed to determine the effect and function of bumetanide on NKCC1 cotransporter in SH-SY5Y cells. Whole-cell currents were recorded in voltage clamp mode with a series of depolarizing voltage steps from -60 mV to +30 mV using a 10 mV step size, for 300 ms of duration.

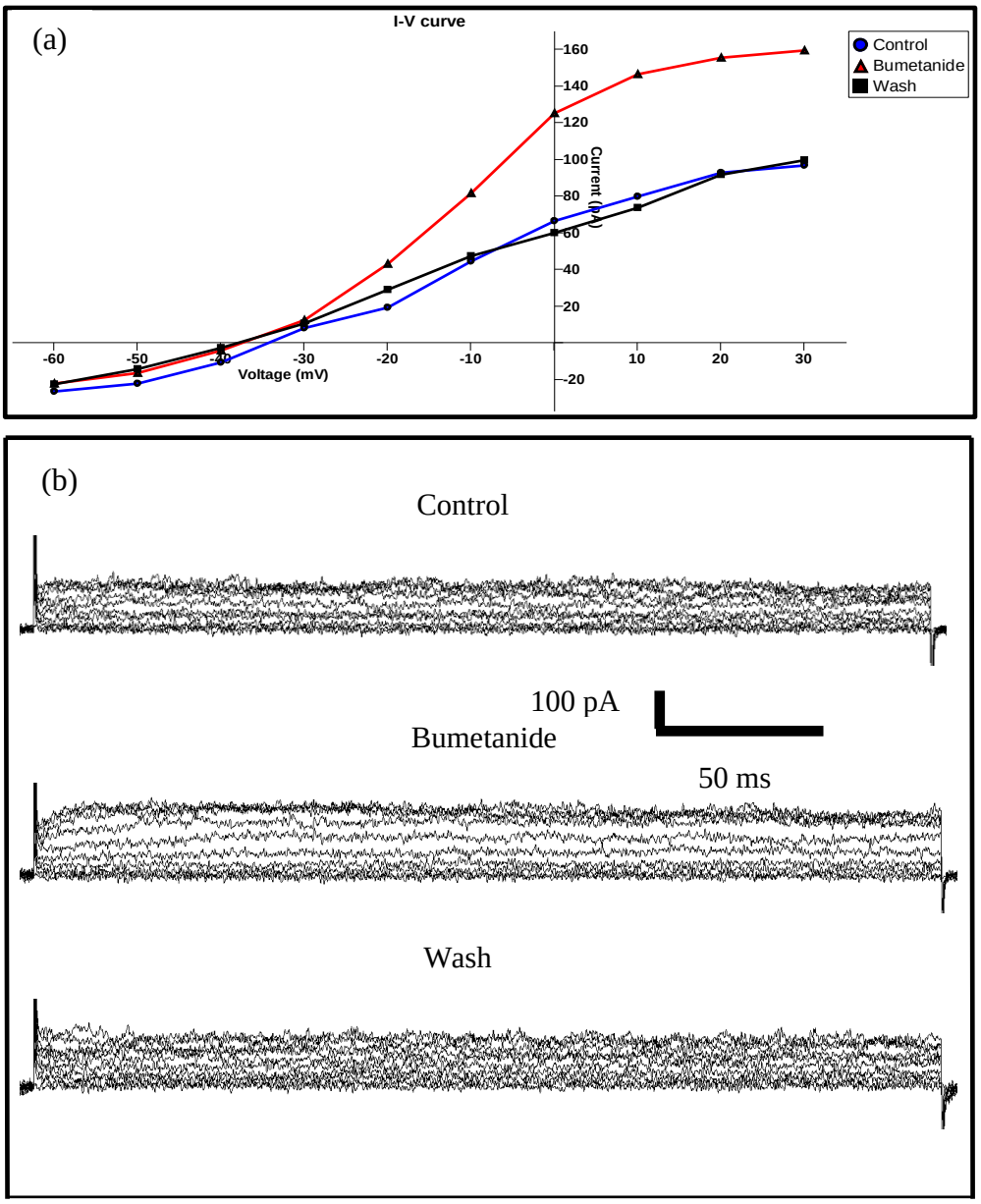

Figure 3.2: Bumetanide induced an increase in potassium currents of SH-SY5Y cells. (a) I-V curves of whole-cell voltage clamp recordings for control, bumetanide (10µM), and wash experiments from a single representative cell. A shift in I-V currents is observed when 10 µM bumetanide is applied. The control and wash I-V curves had almost same current levels at 0 mV voltage, when compared with bumetanide currents. (b) Raw current traces of SH-SY5Y whole-cell K^+ currents stimulated by 300 ms test pulses from -60 mV to +30 mV, in 10mV step increments.

Outward K^+ currents increased when 10 µM bumetanide was perfused for ~10 mins for whole-cell currents were recorded at -60 mV holding potential (Figure 3.2). Following washout of bumetanide the outward K^+ currents recovered to near control levels. So,the outward K^+ currents were reversibly increased by this NKCC1 blocker and 10 µM bumetanide concentration is shown to be effective in inhibiting NKCC1 activity [1]. Bumetanide activates K^+ conductance as shown by increases in K^+ currents, Figures 3.2b (Current traces from one representative cell) and 3.3 (Cumulative I-V curves for 21 cells). I-V curve from a single cell (Figure 3.2 (a)) indicates that a prominent increase in K^+ currents was observed from 0 mV to 30 mV membrane potential range.

The whole-cell currents had a sampling frequency of 10 KHz with an interval of 100 µs and low pass filtered at 1000 Hz using Gaussian type. As shown in Figure 3.2(b), onset of K currents for depolarization test potentials ranging from -60 mV to +30 mV from a holding potential of -60 mV. The I-V curve from a single, representative cell (Figure 3.2 (a)) shows that a prominent increase in K currents was observed for the 0 - 30mV potential range.

As shown in Figure 3.3, the outward potassium currents increased when bumetanide was applied. There was a significant difference in mean values ($P=0.0041$, $n=8$) when the paired Students t-test was performed. Using Clampfit, the current values for corresponding voltage for each cell are noted for control, bumetanide and wash. The mean±SEM curves were then plotted.

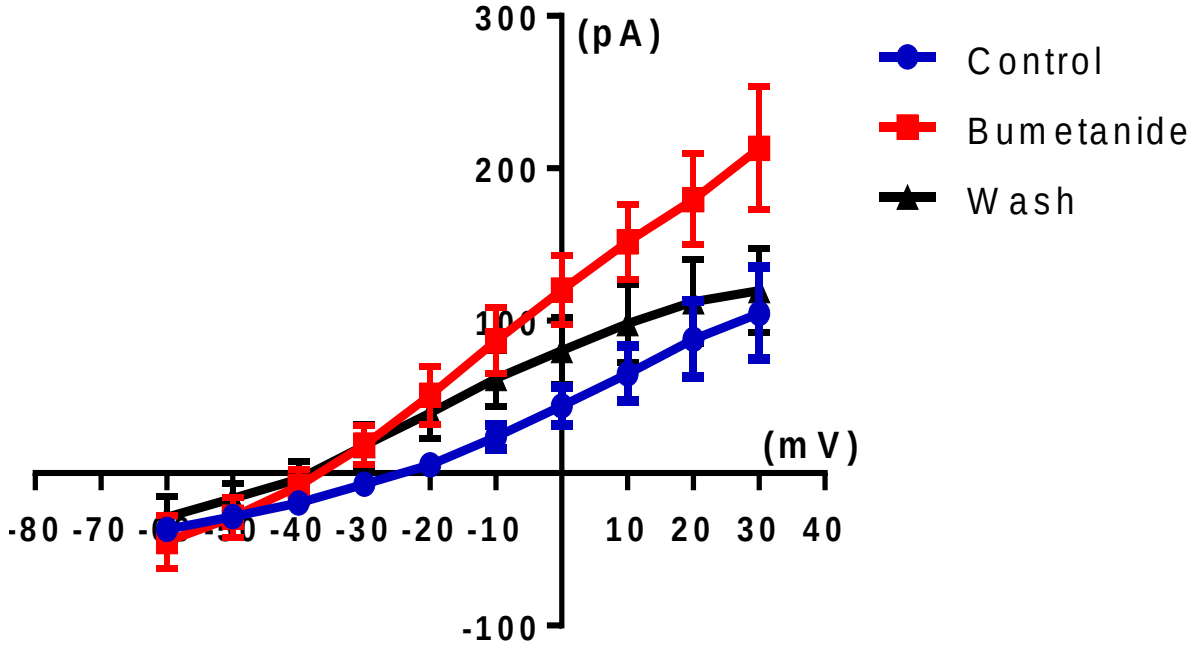

Figure 3.3: I-V curves of SH-SY5Y whole cell recordings (n=8), representing mean current-voltage relations. Current and voltage values were plotted in GraphPad Prism using the data from Clampfit software. At each cell holding potential, mean currents, ±SEM, are displayed for control, bumetanide and wash curves. These data indicate a two-fold increase in potassium currents for bumetanide application when compared to the control. Potassium currents decreased relative to bumetanide for the wash recordings.

3.3 Sensitivity of K^+ Channels to ALD

In order to study the effects of ALD on NKCC1 channels, ECS containing 1 µM ALD was perfused and whole-cell recordings were performed. These recordings were made with continuous perfusion of ECS, and a change in K^+ outward currents was observed after~10 min of ALD application. A single-cell data analysis indicated that there is a reversible increase in outward K currents in response to 1 µM ALD, and further washout of ALD for~15 min revealed recovered current amplitudes. As shown in Figure 3.4(a), I-V relationship curve of a single cell shows the prominent increase in current at -10 – 30 mV holding potentials.

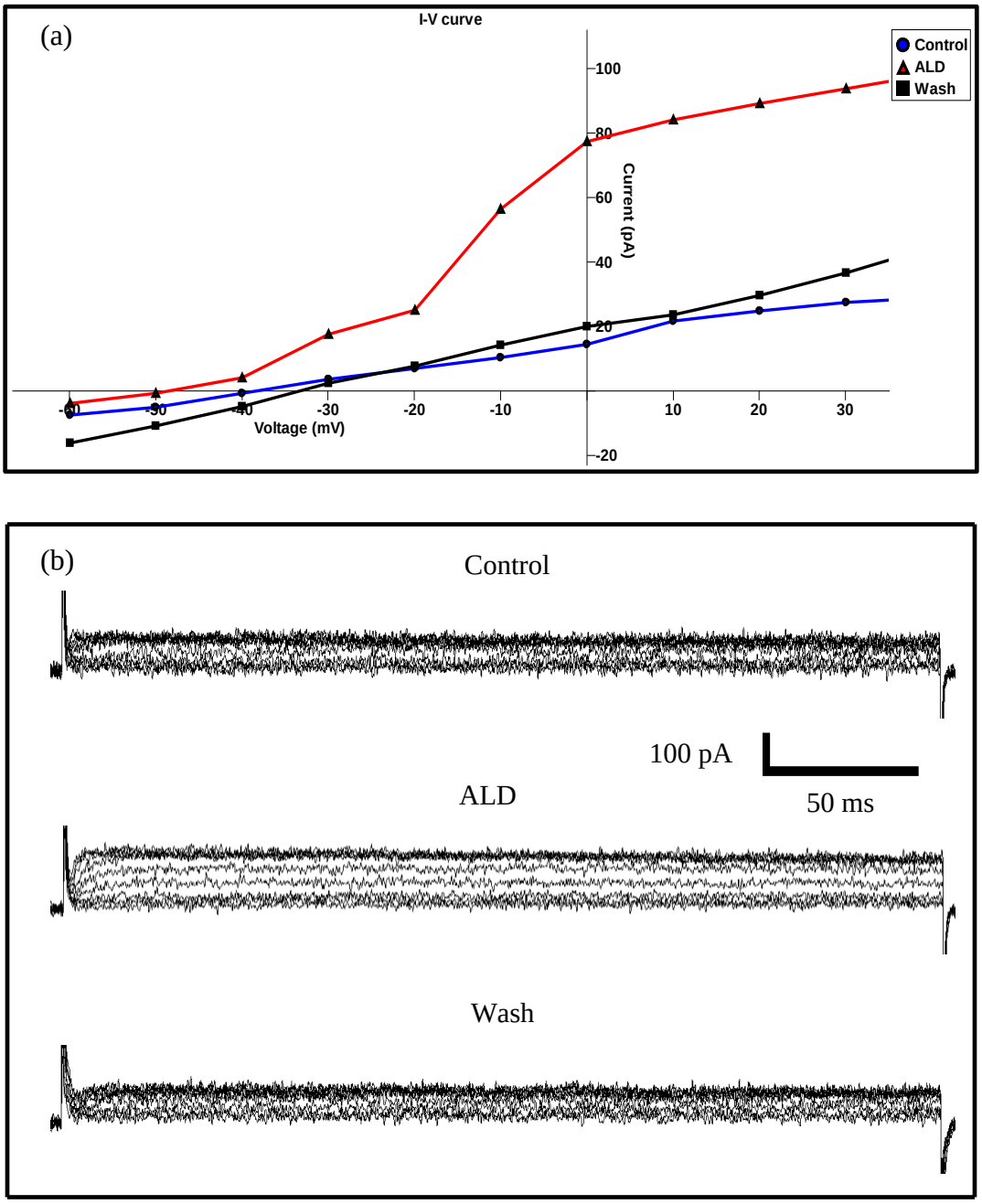

Figure 3.4: Potassium channels in SH-SY5Y cells are sensitive to ALD. (a) I-V curves of whole-cell voltage clamp recordings for control (blue), ALD (red), and wash (black) experiments from a single cell. A shift in I-V currents is observed when 1 µM ALD was applied to cells. The control and wash I-V curves had almost same current levels at 0 mV voltage, when compared with ALD curve. (b) Current traces of SH-SY5Y whole-cell K^+ currents stimulated by 300 ms test pulses from -60 mV to +30 mV holding potentials, in 10mV step increments.

As shown in Figure 3.5, at positive membrane potential, a prominent shift in I-V curves was observed with application of ALD. I/V curves with mean ±SEM from 21 cells provide strong evidence supporting an increase in K^+ currents in SH-SY5Y cells. A paired Student t-test suggest that there is a significant difference (P=0.0027, n=21) between mean values of control and ALD values. The data in Figure 3.5a indicate that the significant onset of the response to ALD was above -30 mv membrane potential, and I-V curve shifted further with additional increases in the membrane potential. K^+ current traces analyzed for single cells when stepping to +30 mV indicate the increases in currents before and after ALD application range from 90.28 pA to 216.70 pA at 50 ms point, as presented in Figure 3.5b.

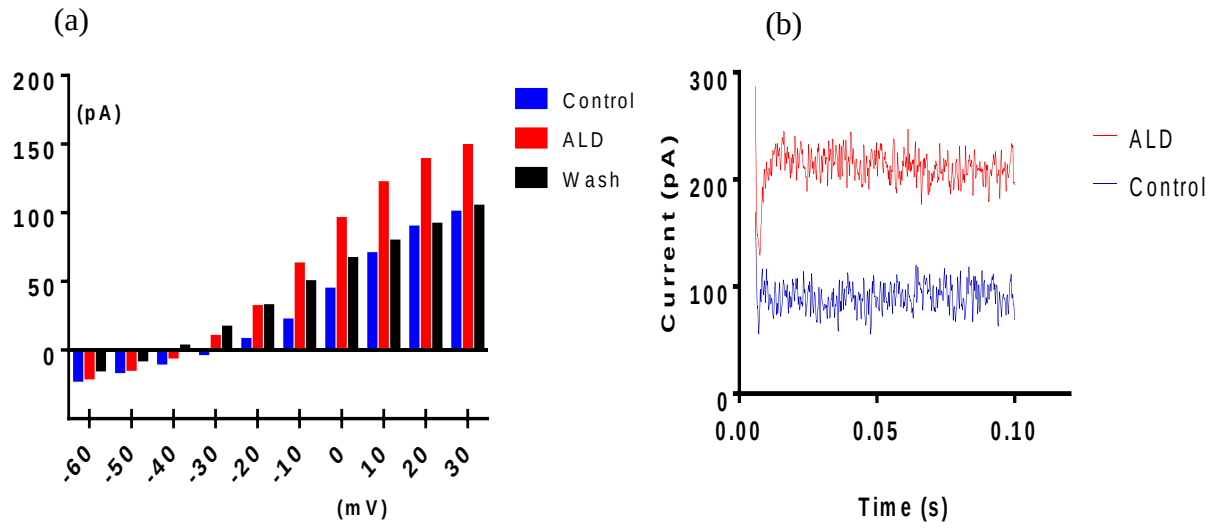

Figure 3.5: K^+ current amplitudes in response to ALD at different cell holding potentials. (a) Mean (n=21) current values plotted across -60 to +30 mV holding potentials show the increase in outward K^+ currents with increases in potential. (b) Single-cell analysis characteristic of K^+ current traces for +30 mV; increases in K^+ currents are clearly observed with application of 1 µM ALD.

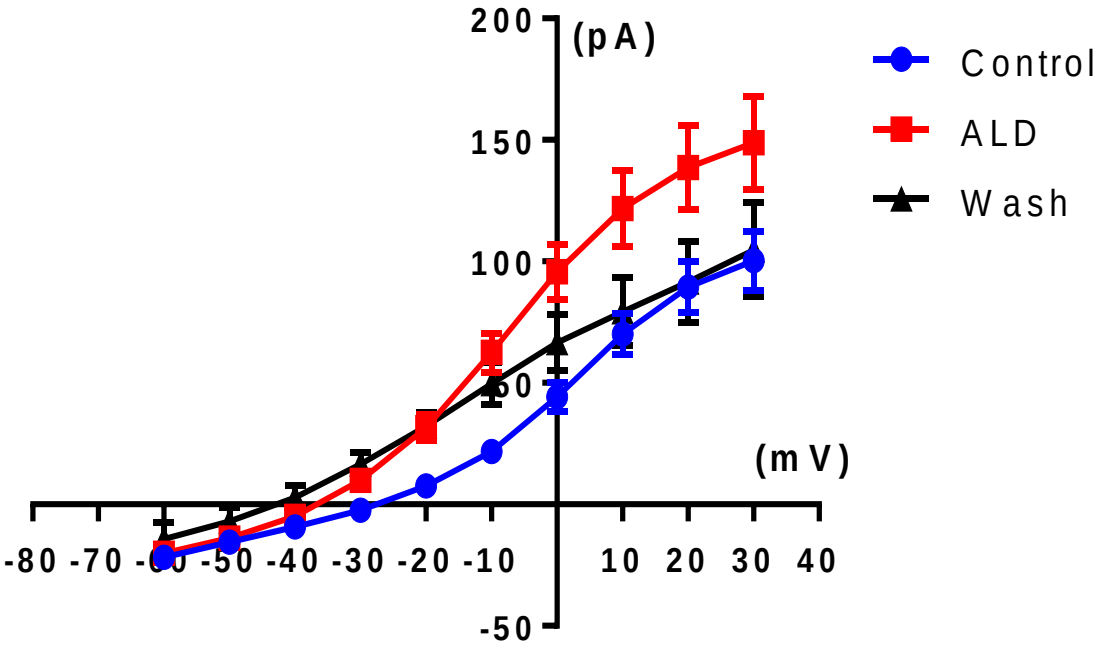

Figure 3.6: I-V curves of SH-SY5Y whole cell recordings (P<0.05, n=21), representing mean current-voltage relations. Current and voltage values were plotted in GraphPad Prism using the data from Clampfit software. At each potential, mean ±SEM is displayed for control (blue), ALD (red) and wash (black) curve. The curves indicate an increase in potassium currents for ALD when compared to controls and washout recordings.

Apart from 1 µM ALD concentration, experiments with 0.1 and 10 µM were also performed and these concentrations resulted in similar I-V trends.

3.4 Discussion

To our knowledge this is the first time the regulatory effects of the hormone ALD have been measured on K^+ channel currents in SH-SY5Y cells. ALD has the ability to upregulate NKCC1 protein expression, linking it to a possible therapeutic targets for improving age-related changes in cochlear physiology [1]. Ding and colleagues first showed that ALD's action on NKCC1 works through mineralocorticoid receptors and related mechanisms, including protein

stabilization [1]. However, the biophysical mechanisms underlying the action of ALD in *in vitro* is not yet known and our initial investigations provide increased understanding of physiological responses of SH-SY5Y cells to ALD. In our initial studies, RT-PCR expression experiments confirmed the presence of NKCC1 co-transporter expression in SH-SY5Y cells. During differentiation of SH-SY5Y cells some unique properties might contribute towards development of different types of channels, such as expression of different channel subunits [21][26]. Interestingly, our findings indicated that both undifferentiated and differentiated SH-SY5Y cells show NKCC1 co-transporter expression. A similar analysis performed by Spitzner et al. illustrates the same expression levels of NKCC1 in differentiated and undifferentiated colon epithelium cells during tumorigenesis [25].

We first investigated the effect of the NKCC1 antagonist bumetanide on SHSY-5Y cells, in order to study the *in vitro* physiological response of the co-transporter. Bumetanide is known to inhibit NKCC1 activity, thereby causing a reduction of intracellular Cl^- concentration [27]. Whole cell recordings in the presence of 10 μM bumetanide showed a significant increase of K^+ currents (from 104.93 ± 30.15 to 213.25 ± 40.15 pA at +30 mV, n=8 before and after application of bumetanide). In agreement with our observations, Wang et al. demonstrated that loop diuretics like bumetanide activate intermediate conductances for Ca^{+2}-activated K^+-channels (IK) and also inhibit NKCC1 co-transporter [27]. There are additional findings that these SH-SY5Y cells lack K_{ATP} channels and that K_{ATP} does not contribute to outward K^+ currents [28, 29]. We believe that the observed increase in K^+ currents with bumetanide application is through activation of voltage-gated K^+ channel and IK channels [28, 30].

SH-SY5Y whole cell current measurements following application of bumetanide provide further indication that NKCC1 might be interacting with the blocker. Molecular studies by Ding

et al. found that ALD sensitively regulates NKCC1 protein expression [1]. Whole-cell current recordings from SH-SY5Y cells in the presence of 1μM ALD showed an outward increase in K^+ currents similar to bumetanide response (from 100.28 ± 12.06 to 148.82 ± 19.17 pA at +30 mV, n=21 before and after application of ALD). A comparison between the mean values of bumetanide and ALD reveals that increases in whole cell currents with bumetanide are higher compared to increases due to ALD (Refer Table 3.1).

Table 3.1: Comparison of mean current values of bumetanide and ALD.

Voltage (mV)	Control (Mean current values)		Drug (Mean current values)	
	Bumetanide (pA) n=8	ALD (pA) n=21	Bumetanide (pA) n=8	ALD (pA) n=21
-60	-36.93	-21.67	-44.76	-20.01
-50	-28.62	-15.5	-28.94	-13.91
-40	-19.4	-9.25	-8.61	-4.95
-30	-7.12	-2.43	18.4	9.81
-20	5.6	7.64	51.29	31.65
-10	23.96	21.69	86.85	62.53
0	44.23	44.31	120.21	95.75
10	65.18	70.15	151.66	121.76
20	87.95	89.51	179.5	138.7
30	104.93	100.28	213.25	148.82

Drug = Bumetanide / ALD, n = number of cells

In marginal cells of the cochlear stria vascularis which produce endolymph, NKCC1 is known to be involved in synergistic transport of K^+ ions into the cochlear duct [31]. Interestingly, our findings from whole-cell current recordings suggest that ALD increases K^+ currents in SH-SY5Y cells. It is also reported that ALD regulates K^+ channels in other physiological systems such as in the lungs, where the hormone ALD has been shown to regulate K^+ channels in the alveolar epithelium [32]. It is also known that ALD increases the basolateral Na^+, K^+-ATPase total activity in renal systems [33]. Our initial data presented in this Thesis reveals additional role of ALD in K^+ currents in neural cells, and further experiments could

provide a better understanding about the effects of ALD on NKCC1 and K^+ channels. Taken together, our studies implicate that bumetanide and ALD regulate K^+ channel currents in human neuroblastoma cells. Identification of specific NKCC1 single channel responses using inside-out patch clamp methodology, that allows for single NKCC1 channels to be isolated, will be a major challenge, since there is need for more evidence on direct measurement of NKCC1 currents.

CHAPTER 4

CONCLUSION

4.1 Summary

We demonstrated for the first time that the NKCC1 ion channels are expressed in both undifferentiated and differentiated SH-SY5Y cells using RT-PCR gene expression techniques. Once we confirmed the presence of NKCC1 in these cells, electrophysiology experiments were conducted to study the actions of bumetanide and ALD on the SH-SY5Y cell physiology. Whole-cell current recordings in the presence of 10 μM bumetanide indicate that this NKCC1 antagonist always induced an *increase* in outward K^+ currents in this cell line. Apart from bumetanide studies, we discovered that ALD helps regulate K^+ channel currents in SH-SY5Y neuroblastoma cells. Whole-cell current data obtained from SH-SY5Y cells when treated with 1 μM ALD reveal this hormone's ability to increase the K^+ channel currents. At this point the exact sequence of events and the intermediate compounds acting in this physiological response are yet to be delineated in more detail. But previous findings in other cells suggest that ALD can regulate K^+ and other channels with different functional effects [32, 33]. Furthermore, bumetanide, being a specific NKCC1 blocker, may increase K^+ currents related to NKCC1. On the other hand, regarding ALD regulatory actions on K^+ channel currents, further experiments could provide a definite understanding of its physiological mechanism of action on NKCC1, and further our knowledge of roles in hearing loss, including ARHL.

4.2 Future Work

We intend to continue our work in investigating the effects of ALD on NKCC1 *in vitro,* to further understand the mechanisms underlying K^+ currents in neural action potential generation. A logical next experiment is to perform siRNA silencing of NKCC1 expression in SH-SY5Y cells and then study the ALD responses. These experiments can provide crucial information on exactly how ALD is acting on NKCC1 channel activity or other cell membrane ion channels crucial for key physiological functions.

REFERENCES

1. Ding, B., et al., *Direct control of Na+-K+-2Cl−-cotransport protein (NKCC1) expression with aldosterone.* American Journal of Physiology - Cell Physiology, 2014. **306**(1): p. C66-C75.

2. Gerelsaikhan, T. and R.J. Turner, *Membrane topology and function of the secretory Na+-K+-2Cl-cotransporter (NKCC1).* Journal of Korean medical science, 2000. **15**(Suppl): p. S3.

3. Moore-Hoon, M.L. and R.J. Turner, *The structural unit of the secretory Na+-K+-2Cl-cotransporter (NKCC1) is a homodimer.* Biochemistry, 2000. **39**(13): p. 3718-3724.

4. Ye, Z.-Y., et al., *NKCC1 upregulation disrupts chloride homeostasis in the hypothalamus and increases neuronal activity–sympathetic drive in hypertension.* The Journal of Neuroscience, 2012. **32**(25): p. 8560-8568.

5. Kahle, K.T., et al., *Roles of the cation–chloride cotransporters in neurological disease.* Nature Clinical Practice Neurology, 2008. **4**(9): p. 490-503.

6. Gates, G.A., N.N. Couropmitree, and R.H. Myers, *GEnetic associations in age-related hearing thresholds.* Archives of Otolaryngology–Head & Neck Surgery, 1999. **125**(6): p. 654-659.

7. Helzner, E.P., et al., *Race and sex differences in age-related hearing loss: The Health, Aging and Body Composition Study.* Journal of the American Geriatrics Society, 2005. **53**(12): p. 2119-2127.

8. SCHUKNECHT, H.F., *Further observations on the pathology of presbycusis.* Archives of otolaryngology, 1964. **80**(4): p. 369-382.

9. Frisina, R.D. and D.R. Frisina, *Physiological and neurobiological bases of age-related hearing loss: biotherapeutic implications.* American journal of audiology, 2013. **22**(2): p. 299-302.

10. Takeuchi, S., M. Ando, and A. Kakigi, *Mechanism generating endocochlear potential: role played by intermediate cells in stria vascularis.* Biophysical Journal, 2000. **79**(5): p. 2572-2582.

11. Sewell, W.F., *The effects of furosemide on the endocochlear potential and auditory-nerve fiber tuning curves in cats.* Hearing research, 1984. **14**(3): p. 305-314.

12. Li, J. and A. Verkman, *Impaired hearing in mice lacking aquaporin-4 water channels.* Journal of Biological Chemistry, 2001. **276**(33): p. 31233-31237.

13. Delpire, E., et al., *Deafness and imbalance associated with inactivation of the secretory Na-K-2Cl co-transporter.* Nature genetics, 1999. **22**(2): p. 192-195.

14. Anselmo, A.N., et al., *WNK1 and OSR1 regulate the Na+, K+, 2Cl− cotransporter in HeLa cells.* Proceedings of the National Academy of Sciences, 2006. **103**(29): p. 10883-10888.

15. Ko, M.C., et al., *Inhibition of NKCC1 Attenuated Hippocampal LTP Formation and Inhibitory Avoidance in Rat.* 2014.

16. Trune, D.R., J. Beth Kempton, and M. Kessi, *Aldosterone (Mineralocorticoid) Equivalent to Prednisolone (Glucocorticoid) in Reversing Hearing Loss in MRL/MpJ-Faslpr Autoimmune Mice.* The Laryngoscope, 2000. **110**(11): p. 1902-1906.

17. Kohn, F.P.M., *Patch clamp experiments with human neuron-like cells under different gravity conditions*, 2010, Institute of Physiology.

18. Kovalevich, J. and D. Langford, *Considerations for the use of SH-SY5Y neuroblastoma cells in neurobiology*, in *Neuronal Cell Culture*. 2013, Springer. p. 9-21.

19. Lotan, R., *Retinoids in cancer chemoprevention.* The FASEB Journal, 1996. **10**(9): p. 1031-1039.

20. Melino, G., et al., *Retinoids and the control of growth/death decisions in human neuroblastoma cell lines.* Journal of neuro-oncology, 1997. **31**(1-2): p. 65-83.

21. Tosetti, P., V. Taglietti, and M. Toselli, *Functional changes in potassium conductances of the human neuroblastoma cell line SH-SY5Y during in vitro differentiation.* Journal of neurophysiology, 1998. **79**(2): p. 648-658.

22. Hamill, O.P., et al., *Improved patch-clamp techniques for high-resolution current recording from cells and cell-free membrane patches.* Pflügers Archiv, 1981. **391**(2): p. 85-100.

23. Veitinger, S., *The Patch-Clamp Technique*. 2011.

24. Matthews, J.B., et al., *Na-K-2Cl cotransporter gene expression and function during enterocyte differentiation. Modulation of Cl-secretory capacity by butyrate.* Journal of Clinical Investigation, 1998. **101**(10): p. 2072.

25. Spitzner, M., *Role of potassium ion channels (K+ channels) on proliferation and development of colonic cancer*, 2008.

26. Swanson, R., et al., *Cloning and expression of cDNA and genomic clones encoding three delayed rectifier potassium channels in rat brain.* Neuron, 1990. **4**(6): p. 929-939.

27. Wang, T., et al., *Bumetanide Hyperpolarizes Madin–Darby Canine Kidney Cells and Enhances Cellular Gentamicin Uptake by Elevating Cytosolic Ca2+ Thus Facilitating Intermediate Conductance Ca2+-Activated Potassium Channels.* Cell biochemistry and biophysics, 2013. **65**(3): p. 381-398.

28. Reeve, H.L., P.F. Vaughan, and C. Peers, *Glibenclamide inhibits a voltage-gated K+ current in the human neuroblastoma cell line SH-SY5Y.* Neuroscience letters, 1992. **135**(1): p. 37-40.

29. Molleman, A., L. Thuneberg, and J. Huizinga, *Characterization of the outward rectifying potassium channel in a novel mouse intestinal smooth muscle cell preparation.* The Journal of physiology, 1993. **470**(1): p. 211-229.

30. Noguchi, T., N. Kamiyama, and M. Kashiwayanagi, *Modulation of voltage-gated ion channels on SH-SY5Y neuroblastoma by non-ionic surfactant, Cremophor EL.* Biological and Pharmaceutical Bulletin, 2010. **33**(12): p. 2013-2017.

31. Quraishi, I.H. and R.M. Raphael, *Computational model of vectorial potassium transport by cochlear marginal cells and vestibular dark cells.* American Journal of Physiology-Cell Physiology, 2007. **292**(1): p. C591-C602.

32. Illek, B., H. Fischer, and W. Clauss, *Aldosterone regulation of basolateral potassium channels in alveolar epithelium.* American Journal of Physiology-Lung Cellular and Molecular Physiology, 1990. **259**(4): p. L230-L237.

33. Summa, V., et al., *Isoform specificity of human Na+, K+-ATPase localization and aldosterone regulation in mouse kidney cells.* The Journal of physiology, 2004. **555**(2): p. 355-364.

APPENDIX A:

I-V CURVES OF WHOLE CELL CURRENT RECORDINGS

A.1 Whole Cell Currents Recordings and I-V Curves

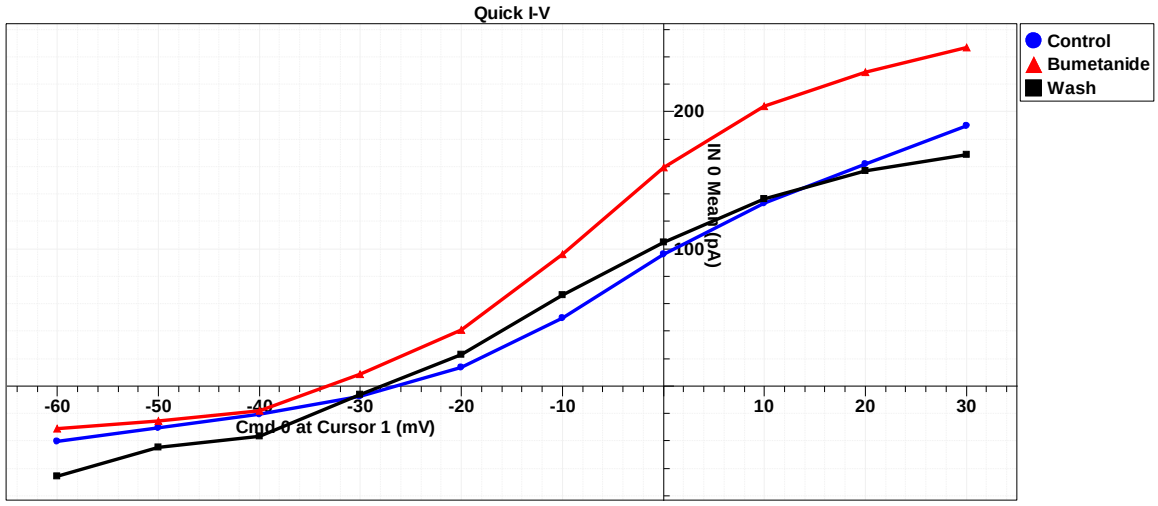

Figure A.1: Representative I-V curve analysis of whole cell current recordings shown in Clampfit.

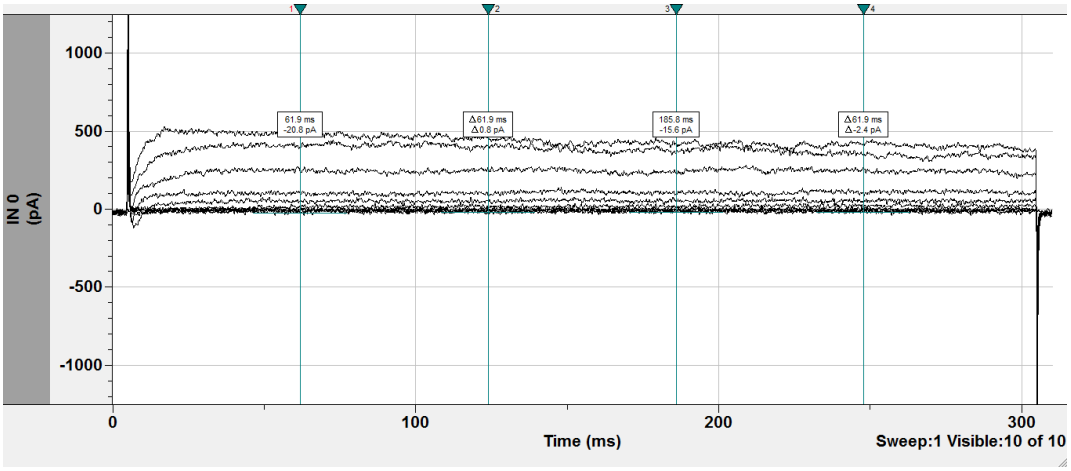

Figure A.2: Representative whole cell currents recording shown in Clampfit.

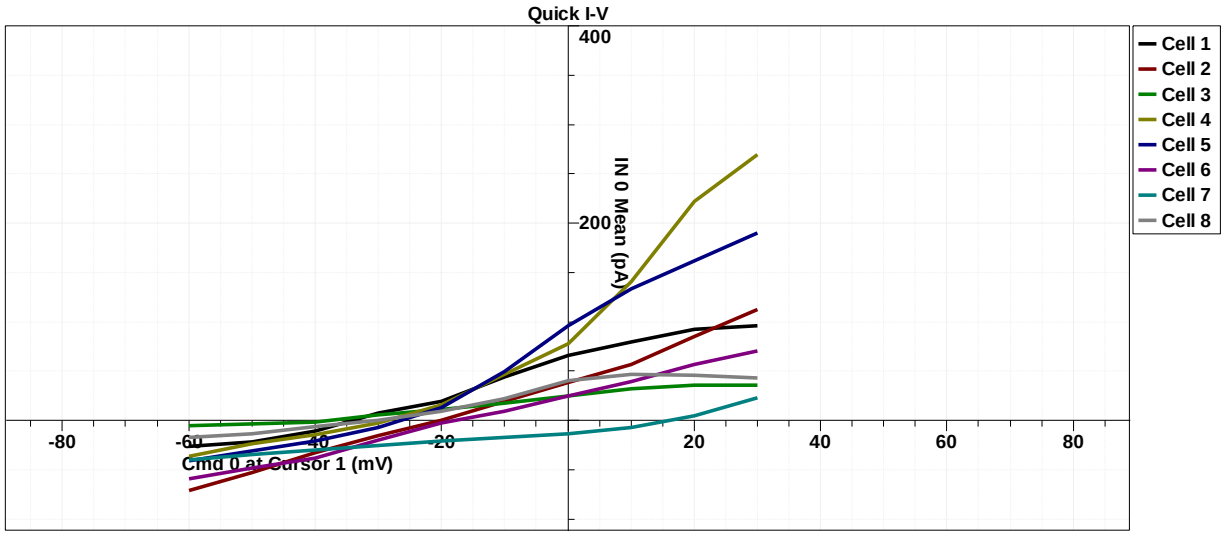

Figure A.3: I-V curves of control whole cell current recordings (n=8).

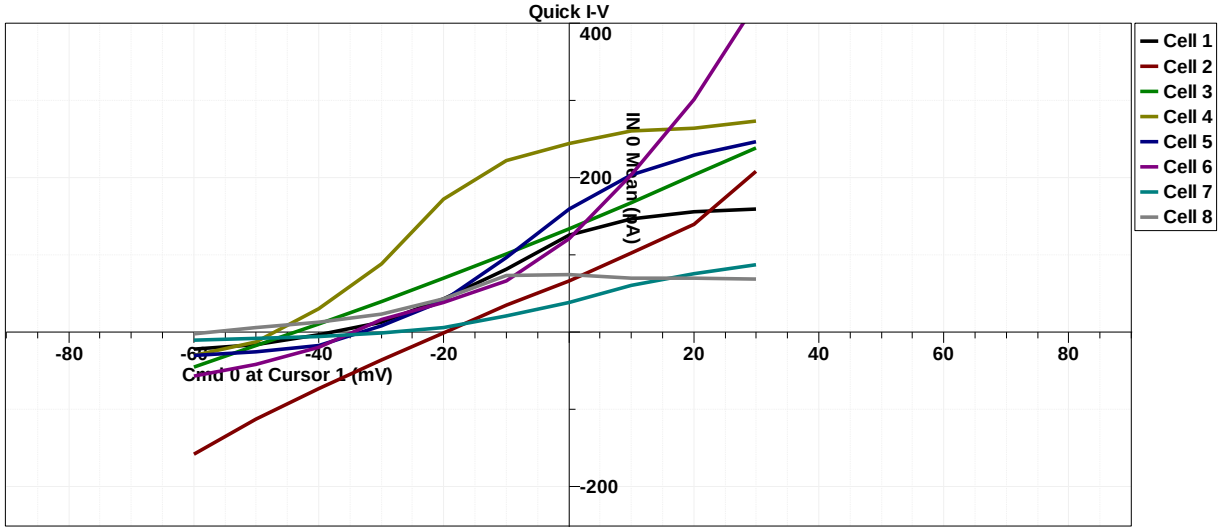

Figure A.4: I-V curves of whole cell current recordings when bumetanide is applied (n=8).

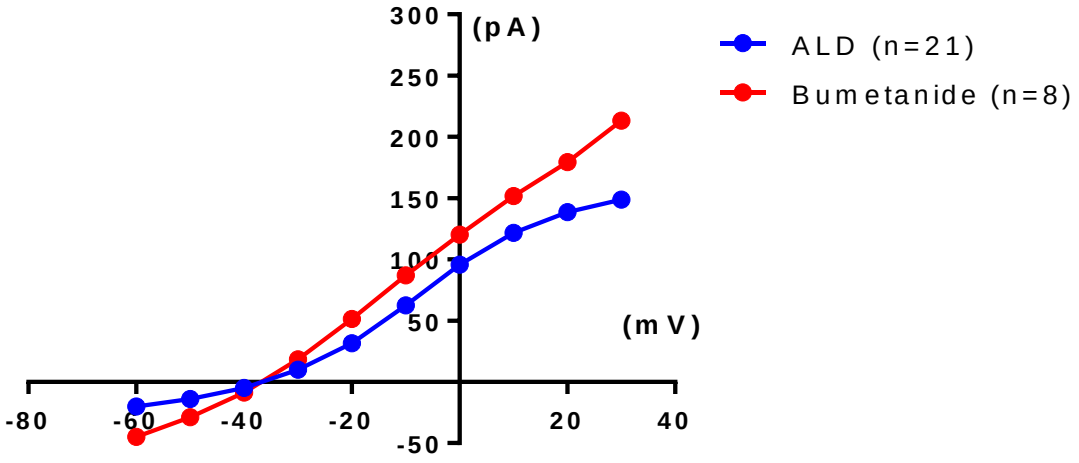

Figure A.5: Mean I-V curves of Bumetanide (n=8) and ALD (n=21) whole cell current recordings.

APPENDIX B:

WHOLE CELL CURRENT RECORDINGS DATA

Table B.1: Current values (pA) recorded at different voltages (mV) before bumetanide application.

Voltage (mV)	Current (pA)							
	Cell1	**Cell 2**	**Cell 3**	**Cell 4**	**Cell 5**	**Cell 6**	**Cell 7**	**Cell 8**
-60	-26.8	-70.9	-5.2	-36.1	-40.7	-58.8	-40.3	-16.8
-50	-22.2	-52.8	-3.4	-23.9	-30.7	-48.3	-34.4	-13.1
-40	-10.9	-32.6	-2.0	-14.9	-20.4	-38.4	-30.1	-6.5
-30	7.9	-15.3	5.6	-2.5	-7.5	-19.6	-25.5	0.0
-20	19.0	0.1	11.4	15.4	13.3	-2.2	-21.2	9.3
-10	44.4	18.9	17.7	46.9	49.7	9.3	-17.2	22.0
0	66.1	38.3	24.7	77.4	95.9	24.4	-13.7	40.8
10	79.5	57.0	32.4	140.8	133.3	39.4	-7.4	46.6
20	92.6	84.9	35.3	221.6	161.7	56.7	4.6	46.2
30	96.4	112.1	35.3	269.2	189.9	70.8	22.7	42.9

Table B.2: Current values (pA) recorded at different voltages (mV) after bumetanide (10 µM) application.

Voltage (mV)	Current (pA)							
	Cell1	**Cell 2**	**Cell 3**	**Cell 4**	**Cell 5**	**Cell 6**	**Cell 7**	**Cell 8**
-60	-22.4	-158.6	-46.1	-30.0	-30.9	-56.8	-11.1	-2.3
-50	-16.5	-113.5	-17.4	-13.4	-25.8	-41.7	-8.6	5.5
-40	-4.3	-73.0	10.2	29.8	-17.8	-20.0	-6.3	12.6
-30	12.1	-36.9	38.8	87.9	8.4	16.3	-1.8	23.0
-20	42.7	-1.5	69.3	172.1	40.8	38.0	6.1	43.0
-10	81.4	34.5	101.2	222.1	96.3	66.4	20.3	72.6
0	124.9	66.6	133.2	243.6	159.2	121.3	38.4	74.5
10	146.3	101.7	167.5	260.5	203.8	203.1	60.3	70.1
20	155.2	139.9	202.8	263.3	228.8	301.1	75.0	70.0
30	159.2	207.5	238.6	273.0	246.8	425.2	87.4	68.3

Table B.3: Current values (pA) recorded at different voltages (mV) before ALD application.

Voltage (mV)	Current (pA)																				
	Cell1	**Cell 2**	**Cell 3**	**Cell 4**	**Cell 5**	**Cell 6**	**Cell 7**	**Cell 8**	**Cell 9**	**Cell 10**	**Cell 11**	**Cell 12**	**Cell 13**	**Cell 14**	**Cell 15**	**Cell 16**	**Cell 17**	**Cell 18**	**Cell 19**	**Cell 20**	**Cell 21**
-60	11.0	-45.1	-37.5	-32.0	-26.6	-34.1	-40.3	-16.8	0.0	-2.5	-21.6	-10.8	-7.4	-34.1	-59.3	-7.6	-7.7	-18.9	-1.0	-15.2	-47.7
-50	16.3	-29.6	-29.8	-25.3	-20.2	-24.3	-34.4	-13.1	3.2	0.0	-14.9	-5.7	-4.1	-24.1	-46.8	-5.0	-6.7	-13.6	-0.8	-10.0	-36.4
-40	19.8	-14.0	-24.1	-16.9	-13.9	-14.0	-30.1	-6.5	6.3	2.8	-7.2	-2.1	-1.4	-16.3	-37.0	-0.8	-3.6	-9.3	0.5	-5.4	-21.3
-30	24.1	4.0	-16.3	-4.0	-6.3	-4.9	-25.5	0.0	10.5	6.3	-0.3	2.5	1.4	-6.8	-26.9	3.5	-1.0	-4.7	4.7	-0.2	-11.3
-20	30.4	33.2	-7.1	17.0	5.7	6.3	-21.2	9.3	22.0	11.9	10.8	11.5	5.0	9.6	-15.4	7.0	2.1	-0.3	9.3	6.1	7.4
-10	33.1	62.5	9.8	41.9	20.4	15.8	-17.2	22.0	36.0	18.4	26.3	26.5	8.3	49.4	-1.4	10.4	12.9	5.1	27.8	22.1	25.4
0	35.3	76.1	43.9	92.0	49.7	26.8	-13.7	40.8	60.9	32.9	57.5	64.0	10.6	104.5	14.3	14.5	46.7	17.3	55.2	52.8	48.7
10	42.3	94.3	83.5	154.9	95.0	33.2	-7.4	46.6	72.6	70.7	106.2	101.2	13.6	115.1	28.7	21.6	101.1	55.0	91.4	79.1	74.4
20	49.6	122.9	113.3	190.5	144.2	41.7	4.6	46.2	78.0	96.5	144.3	105.5	16.4	117.3	35.6	24.8	125.8	114.1	125.1	86.0	97.2
30	53.0	138.0	143.6	211.1	183.1	50.9	22.7	42.9	78.7	106.8	171.0	111.6	18.4	107.0	45.0	27.4	126.8	139.7	138.1	84.7	105.6

Table B.4: Current values (pA) recorded at different voltages (mV) after ALD (1 µM) application.

Voltage (mV)	Current (pA)																			
	Cell1	Cell 2	Cell 3	Cell 4	Cell 5	Cell 6	Cell 7	Cell 8	Cell 9	Cell 10	Cell 11	Cell 12	Cell 13	Cell 14	Cell 15	Cell 16	Cell 17	Cell 18	Cell 19	Cell 20	Cell 21
-60	-26.6	-74.9	-40.4	-22.0	-4.1	-2.2	-6.1	-2.3	-1.2	-10.6	-16.3	-21.7	-17.2	-20.8	-29.0	-4.0	-12.5	-24.7	-16.6	-7.3	-59.9
-50	-19.7	-47.1	-29.8	-16.3	4.8	0.4	-3.6	5.5	-0.1	-7.5	-13.3	-17.5	-13.9	-14.3	-22.7	-0.7	-9.0	-20.4	-14.4	-5.3	-47.3
-40	-7.2	-16.1	-19.8	-10.8	21.9	9.2	1.0	12.6	4.6	1.4	-8.0	-7.2	-8.4	-2.5	-16.5	3.9	-6.0	-16.4	-11.9	-2.1	-25.6
-30	17.9	24.0	-11.3	9.6	52.8	16.6	10.0	23.0	9.0	19.0	16.7	0.4	0.6	23.0	-7.5	17.6	4.5	-10.6	-7.4	10.7	-12.3
-20	75.2	65.4	0.3	38.0	99.2	32.4	25.4	43.0	20.7	38.1	52.5	6.4	14.2	44.3	14.6	24.9	23.1	6.2	-1.5	26.2	16.2
-10	135.5	109.6	26.8	90.2	134.6	56.3	40.6	72.6	37.0	80.7	91.3	10.0	42.8	95.0	39.0	56.3	71.2	26.1	13.4	48.7	35.8
0	164.8	153.0	70.6	208.8	156.9	63.5	57.4	74.5	52.6	149.6	140.7	16.9	63.7	131.8	63.7	77.2	131.5	64.6	37.9	83.3	47.5
10	168.1	200.0	111.6	322.5	162.5	58.8	68.2	70.1	53.0	196.1	181.4	25.9	68.3	142.1	105.0	84.0	185.6	144.9	51.9	103.1	54.0
20	176.5	254.4	146.4	336.9	175.2	57.3	78.7	70.0	56.0	215.0	199.4	45.0	75.7	125.5	141.0	89.0	195.0	237.0	69.0	102.8	66.9
30	179.5	300.9	167.7	345.1	191.8	53.8	81.5	68.3	55.6	232.1	204.1	66.8	78.4	119.7	144.9	93.8	196.0	291.7	79.3	99.7	74.4

APPENDIX C:

CUMULATIVE DATA GRAPHS

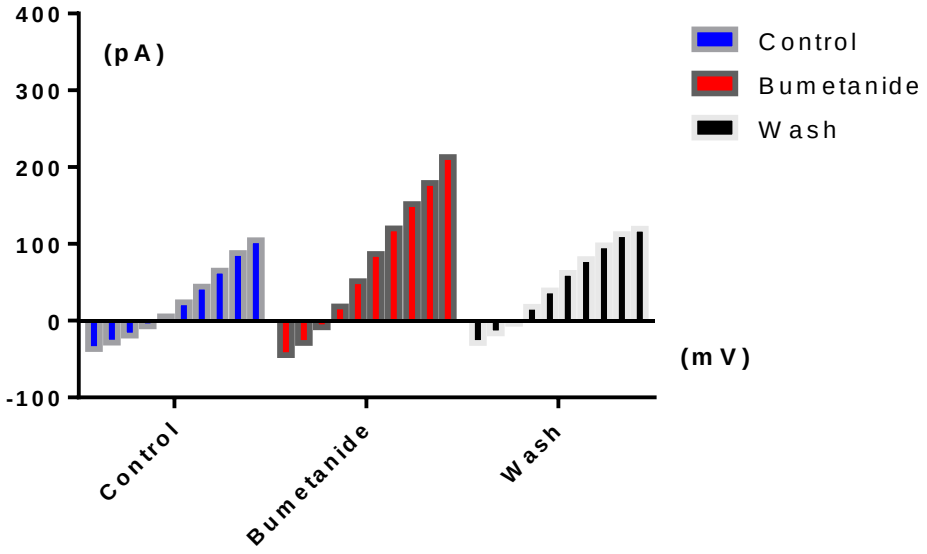

Figure C.1: Cumulative (n=8) grouped graph for control, bumetanide and wash data.